CHAPTER V
INFLUENCE OF MOLECULAR CHARACTERISTICS ON NON-ISOTHERMAL MELT-CRYSTALLIZATION KINETICS OF SYNDIOTACTIC POLYPROPYLENE

5.1 Abstract

Non-isothermal melt-crystallization and subsequent melting behavior for six syndiotactic polypropylene (sPP) resins having different molecular characteristics were investigated by differential scanning calorimetry (DSC). For a given sPP resin, the crystallization exotherm became wider and shifted towards a lower temperature with increasing cooling rate. Among all of the sPP resins investigated, the crystallization exotherm of sPP#11 was found to locate at the highest temperature range, followed by that of sPP#14, sPP#10, sPP#13, sPP#12, and sPP#9, respectively. Based on the absolute temperature scale, sPP#11 showed the highest tendency to start crystallizing during a cooling scan. The ability of these resins to start crystallizing was found to be very similar when the difference in the equilibrium melting temperature of the resins was taken into account. The non-isothermal melt-crystallization kinetics of these sPP resins was well described by the Avrami, Urbanovici–Segal, Ozawa, and Ziabicki models. The subsequent melting behavior of these sPP resins exhibited either a single melting endotherm or double melting endotherms.

5.2 Introduction

After the Ziegler–Natta catalyst had been introduced in the middle of the 1950s, the isotactic form of polypropylene (iPP) was successfully synthesized in 1958. Two years later, the syndiotactic form of the same polymer was successfully synthesized [1,2] using the same type of catalyst system, but the resulting polymer contained a considerable amount of both stereo and regio-irregular defects. In 1988, production of

highly stereo- and regio-regular syndiotactic polypropylene (sPP) was realized with the advent of the metallocene catalyst system [3]. This led to a renewed interest on this polymer. Some prospective uses for sPP in the industries are, for examples, in film [4,5], injection molding [6], and melt-spun fiber [7,8] applications.

It is generally known that physical and mechanical properties of a semi-crystalline polymer are dictated by morphology, which, in turn, is influenced by crystallization behavior of the polymer. Crystallization behavior is strongly influenced by molecular characteristics (e.g. molecular weight averages, molecular weight distribution, stereo-regularity, etc.) of the crystallizing polymer and the processing conditions. It is, therefore, of interest to study the effects of molecular characteristics on crystallization kinetics of a semi-crystalline polymer, which is a key to determine the final properties of a polymeric product.

In the present contribution, differential scanning calorimetry (DSC) was used to study non-isothermal melt-crystallization and subsequent melting behavior of sPP resins of different molecular characteristics. The kinetics of the non-isothermal melt-crystallization process was analyzed based on various macrokinetic models, i.e. the Avrami, Urbanovici–Segal, Ozawa, and Ziabicki models. The activation energy for nonisothermal melt-crystallization process of these resins was also evaluated based on the differential iso-conversional method of Friedman.

5.3 Theoretical Background

In DSC, the energy released during a nonisothermal crystallization process appears to be a function of temperature rather than of time, as in the case of isothermal crystallization process. As a result, the relative crystallinity as a function of temperature $\theta(T)$ can be formulated as

$$\theta(T) = \frac{\int_{T_0}^{T} (\mathrm{d}H_c/\mathrm{d}T)\mathrm{d}T}{\Delta H_c},$$

(5.1)

where T_0 and T represent the onset and an arbitrary temperature, respectively, dH_c is the enthalpy of crystallization released during an infinitesimal temperature range dT, and ΔH_c is the total enthalpy of crystallization for a specific cooling condition.

To use Eq. (5.1) in analyzing non-isothermal crystallization data obtained by DSC, it is assumed that the sample experiences a similar thermal history as designated by the DSC furnace. This can only be realized when the difference between the temperatures of the sample and the furnace is minimal. If this condition is valid, the relation between the crystallization time t and the sample temperature T can be written as

$$t = \frac{T_0 - T}{\phi}, \tag{5.2}$$

where T_0 is an arbitrary reference temperature and ϕ is the cooling rate. According to Eq. (5.2), the horizontal temperature axis observed in a DSC thermogram for the non-isothermal crystallization data can be transformed into the time domain.

The most common approach to describe the overall isothermal crystallization kinetics is the Avrami model [9–11], in which the relative crystallinity as a function of time $\theta(t)$ can be expressed as

$$\theta(t) = 1 - \exp\left(-\left(K_A t\right)^{n_A}\right) \in [0,1], \tag{5.3}$$

where K_A and n_A are the Avrami crystallization rate constant and the Avrami exponent, respectively. Both K_A and n_A are constants specific to a given crystalline morphology and type of nucleation for a particular crystallization condition [12]. It should be noted that the units of K_A are given as an inverse of time. Although the Avrami equation is often used to describe the isothermal crystallization behavior of semi-crystalline

polymers, it has also been applied to describe the non-isothermal crystallization behavior of semi-crystalline polymers [13,14].

Urbanovici and Segal [15] modified the Avrami model and proposed a new kinetic equation in the following form:

$$\theta(t) = 1 - \left[1 + (r-1)(K_{US}t)^{n_{US}}\right]^{1/(1-r)} \in [0,1],$$

(5.4)

where K_{US} and n_{US} are the Urbanovici–Segal rate constant and the Urbanovici–Segal exponent, respectively, and r is a parameter which satisfies the condition $r > 0$. When the value of r approaches 1, the Urbanovici–Segal equation becomes identical to the Avrami equation. This simply means that the parameter r is merely a factor determining the degree of deviation of the Urbanovici–Segal model from the Avrami model. It is noted that the Urbanovici–Segal kinetic parameters have a similar physical meaning to the Avrami kinetic parameters and the units of K_{US} are also given as an inverse of time.

Based on the mathematical derivation of Evans [16], Ozawa extended the Avrami theory to describe nonisothermal crystallization by assuming that the sample was cooled with a constant rate from the molten state [17]. In the Ozawa method, the time variable in the Avrami equation was replaced by a cooling rate, resulting in the relative crystallinity as a function of temperature $\theta(T)$ to be able to be expressed as a function of cooling rate ϕ as

$$\theta(T) = 1 - \exp\left[-\left(\frac{K_O}{\phi}\right)^{n_O}\right] \in [0,1],$$

(5.5)

where K_O and n_O are the Ozawa crystallization rate constant and the Ozawa exponent, respectively. Both of the Ozawa kinetic parameters hold a similar physical meaning to those of the Avrami ones.

Instead of describing the crystallization process with complicated mathematical models, Ziabicki [18–20] proposed that the kinetics of polymeric phase transformation can be described by a first-order kinetic equation of the form:

$$\frac{d\,\theta(t)}{dt} = K_z(T)[1 - \theta(t)],$$

(5.6)

where $K_Z(T)$ is a temperature-dependent crystallization rate function. In the case of non-isothermal crystallization, both $\theta(t)$ and $K_Z(T)$ functions vary and are dependent on the cooling rate used. For a given cooling or heating condition, Ziabicki [18–20] showed that the crystallization rate function $K_Z(T)$ can be described by a Gaussian function of the form:

$$K_z(T) = K_{Z,\max} \exp\left[-4\ln 2\frac{(T - T_{\max})^2}{D^2}\right],$$

(5.7)

where $T_{\max}$ is the temperature at which the crystallization rate is maximum, $K_{Z,\max}$ is the crystallization rate at $T_{\max}$, and D is the width at half-height of the crystallization rate function. Based on the iso-kinetic approximation, integration of Eq. (5.7) over the whole crystallizable range (i.e. $T_g < T < T_m^0$) leads to an important characteristic value describing the crystallization ability of semi-crystalline polymers, i.e. the kinetic crystallizability index G_Z:

$$G_Z = \int_{T_g}^{T_m^0} K_z(T)dT \approx 1.064 K_{Z,\max} D,$$

(5.8)

According to the approximate theory [18], the parameter G_Z describes the ability of semi-crystalline polymers to crystallize when it is cooled at unit cooling rate from the molten state [20].

In the case of non-isothermal crystallization studies using DSC, Eq. (5.8) can be applied only when the crystallization rate function $K_Z(T)$ is replaced with a temperature-derivative of the relative crystallinity as a function of temperature [i.e. $(d\theta/dT)_\phi$] specific for each cooling rate studied. As a result, Eq. (5.8) becomes

$$G_{Z,\phi} = \int_{T_g}^{T_m^0} (d\theta/dT)_\phi \approx 1.064 (d\theta/dT)_{\phi,\max} D_\phi , \qquad (5.9)$$

where $(d\theta/dT)_{\phi,\max}$ and D_ϕ are the maximum crystallization rate and the width at half-height of the $(d\theta/dT)_\phi$ function. According to Eq. (5.9), $G_{Z,\phi}$ is the kinetic crystallizability index for an arbitrary cooling rate ϕ. The Ziabicki kinetic crystallizability index G_Z can be finally obtained by normalizing $G_{Z,\phi}$ with ϕ (i.e. $G_Z = G_{Z,\phi}/\phi$).

For non-isothermal crystallization of semi-crystalline polymers, reliable values of the effective energy barrier can be obtained, for example, by the differential iso-conversional method of Friedman [21] or by the integral iso-conversional method of Vyazovkin [22–24]. In this work, the Friedman method was used, due largely to the reliability and simplicity of the method [23,24]. The Friedman equation is expressed as

$$\ln[\dot{\theta}_\theta(t)] = A - \frac{\Delta E_\theta}{RT} , \qquad (5.10)$$

where $\dot{\theta}_\theta(t)$ is the instantaneous crystallization rate for a given value of relative crystallinity θ, A is an arbitrary pre-exponential parameter, and ΔE_0 is the effective energy barrier of the process for a given θ. By plotting $\dot{\theta}_\theta(t)$ obtained for various cooling rates against the corresponding inverse of temperature for a given θ, the

effective energy barrier for non-isothermal crystallization process can be finally determined.

5.4 Experimental

5.4.1 Materials

Six sPP resins (i.e. internal codes: sPP#9 to sPP#14) of various molecular characteristics (see Table 5.1) were synthesized with two different metallocene catalyst systems. Resins sPP#9 to sPP#11 were synthesized with isopropylidene (cyclopentadienyl)(9-fluorenyl)zirconium dichloride using MMAO as the activator (with the Al/Zr ratio being 2000) in bulk monomer at 70, 50, and 30°C, respectively. Resins sPP#12 to sPP#14 were synthesized with diphenylmethylidene(cyclopentadienyl)(9-fluorenyl)zirconium dichloride using MMAO as the activator (with the Al/Zr ratio being 2000) in bulk monomer at 70, 50, and 30°C, respectively. The as-polymerized polymers were de-ashed via a solvent/non-solvent liquid–liquid extraction and subsequently stabilized with an antioxidant. The de-ashed/stabilized polymers were characterized for their molecular weight averages using size-exclusion chromatography (SEC) and their tacticity using ^{13}C-nuclear magnetic resonance (NMR), from which the results are summarized in Table 5.1.

5.4.2 Sample Preparation

The as-polymerized resins were compressed into films by placing the resins between a pair of transparency films, which were later sandwiched between a pair of stainless steel platens in a Wabash V50H compression press. The thickness of the films was 100 ± 10 μm. After being pre-heated at 190°C for 2 min, the films were melt-pressed at 190°C for another 2 min under an applied clamping force of 5 tons. The compression-molded films were then cooled to 40°C in the compression press. The cooling of the platens was achieved by running cold water through channels in the press platens and was fitted well by an exponential decay with a time constant of 3 min.

Table 5.1 Molecular characteristics of sPP# 9 to sPP#14 and the estimated equilibrium melting temperature (T_m^0) based on linear Hoffman-Weeks extrapolative method

Resin	Mw	Mw/Mn	Racemic dyad	Racemic pentad
			[%r]	[%rrrr]
sPP#9	99,000	2.1	90.8	78.0
sPP#10	136,000	2.2	91.9	80.3
sPP#11	188,000	2.3	92.5	83.0
sPP#12	407,000	3.3	91.4	78.9
sPP#13	606,000	3.2	92.8	83.4
sPP#14	952,000	2.5	95.1	87.8

Resin	Triad Analysis of Data			T_m^0 (°C)
	%isotactic	%atactic	%syndiotactic	
sPP#9	3.3	8.3	88.4	144.2
sPP#10	2.2	7.9	89.9	156.0
sPP#11	2.3	7.3	90.4	159.7
sPP#12	2.6	7.7	89.7	142.3
sPP#13	2.2	7.0	90.8	151.1
sPP#14	1.2	5.2	93.6	157.0

5.4.3 Differential Scanning Calorimetry Measurements

A Perkin–Elmer Series 7 differential scanning calorimeter (DSC) was used to record non-isothermal melt-crystallization exotherms and subsequent melting endotherms for these resins. Calibration for the temperature scale was carried out using an indium standard ($T_m^0 = 156.6$°C and $\Delta H_f^0 = 28.5$ J g^{-1}) on every other run. To minimize thermal lag between the polymer sample and the DSC furnace, each sample holder was loaded with a disc-shaped sample, cut from the as-prepared films, and each one weighed around 3.6 ± 0.4 mg. Each sample was used only once and all the runs were carried out under nitrogen atmosphere to minimize thermal degradation.

The experiment started with heating each sample from 25 to 190°C at a heating rate of 80°C min^{-1}, in order to set a similar thermal history to all of the samples

investigated. To ensure complete melting, each sample was melt-annealed at 190°C for 5 min [25,26], after which the sample was cooled at the desired cooling rate ϕ, ranging from 5 to 40°C min^{-1}, to 25°C. The subsequent melting behavior was then observed by reheating the sample at a heating rate of 20°C min^{-1} to 165°C. Both non-isothermal melt-crystallization exotherms and subsequent melting endotherms were recorded for further analysis.

5.5 Results and Discussion

5.5.1 Non-Isothermal Melt-Crystallization and Subsequent Melting Behavior
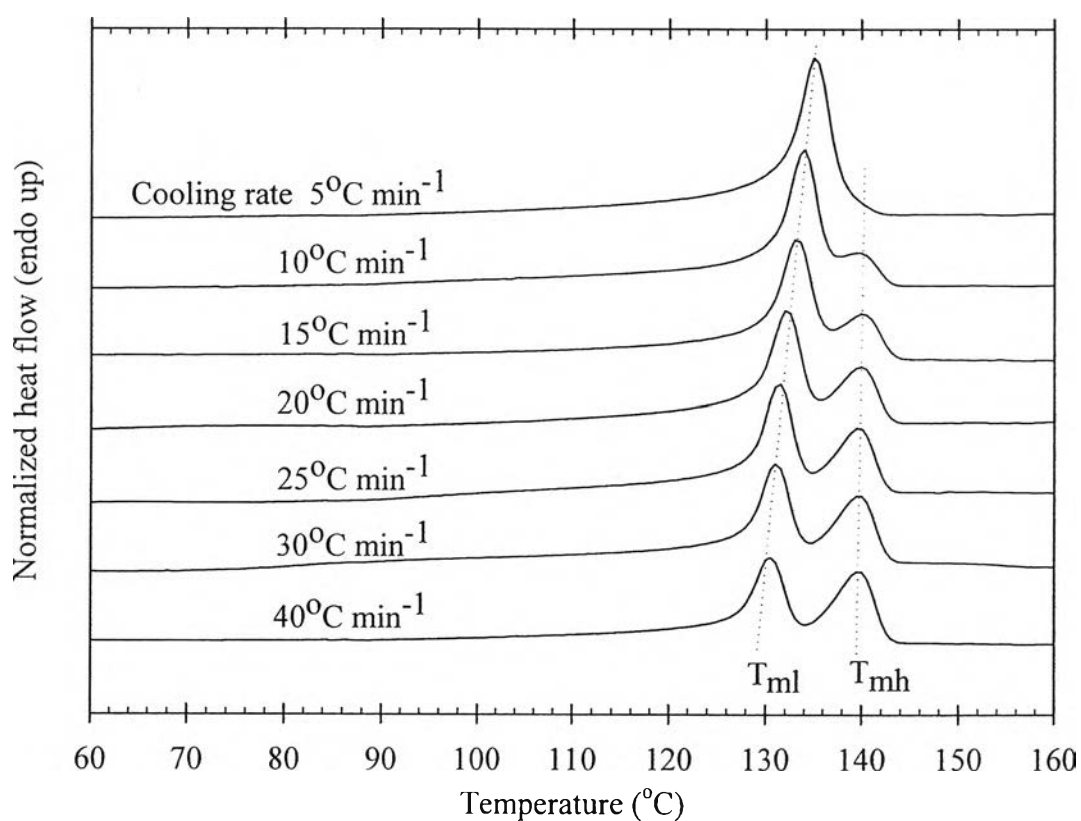
Fig. 5.1 shows non-isothermal melt-crystallization exotherms and subsequent melting endotherms of sPP#10 for seven different cooling rates, ranging from 5 to 40°C min^{-1}. Clearly, a single crystallization exotherm was observed for each cooling and the exothermic trace became wider and shifted towards a lower temperature with increasing cooling rate used (see Fig. 5.1(a)), as it normally would for crystallization in a nucleation-controlled region. Other sPP resins also exhibited a similar behavior to that observed for sPP#10. In order to obtain quantitative kinetic information, these crystallization exotherms had to be converted to the relative crystallinity as a function of temperature $\theta(T)$ using Eq. (5.1). Based on these $\theta(T)$ curves (the results not shown), some kinetic data [e.g. the temperature at 1% relative crystallinity $T_{0.01}$, the temperature at the maximum crystallization rate (i.e. peak temperature) T_p, and the temperature at 99% relative crystallinity $T_{0.99}$] can be obtained and the values of these parameters for all the sPP resins studied are summarized in Table 5.2. Apparently, the $T_{0.01}$, T_p , and $T_{0.99}$ values were all shifted towards lower temperatures with increasing cooling rate. It should be noted that both $T_{0.01}$ and $T_{0.99}$ values represent the apparent onset and ending temperatures of the non-isothermal melt-crystallization process.
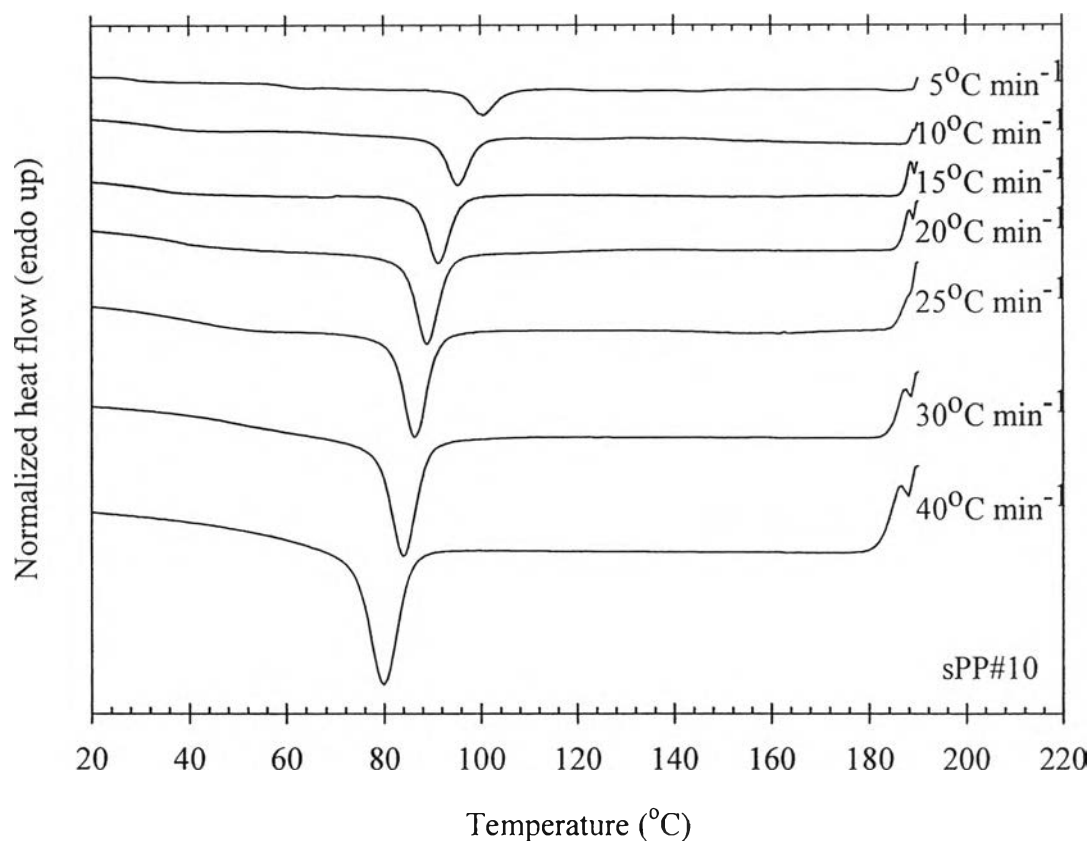
Figure 5.1(a) Non-isothermal melt-crystallization exotherm of sPP#10 observed for seven different cooling rates, ranging from 5 to 40°C min^{-1}.

Based on the $T_{0.01}$, T_p , and $T_{0.99}$ values listed in Table 5.2, it can be deduced that the crystallization exotherm of sPP#11 for any given cooling rate was found to locate at the highest temperature range when comparing with other sPP resins investigated, followed by that of sPP#14, sPP#10, sPP#13, sPP#12, and sPP#9 resin, respectively. Without knowledge of the equilibrium melting temperature T_m^0 of these sPP resins, these observations may lead to a wrong impression that sPP#11 had the highest ability to start crystallizing during a cooling scan in comparison with other sPP resins. Since these sPP resins have a different value of T_m^0 (see Table 1, as well as Ref.
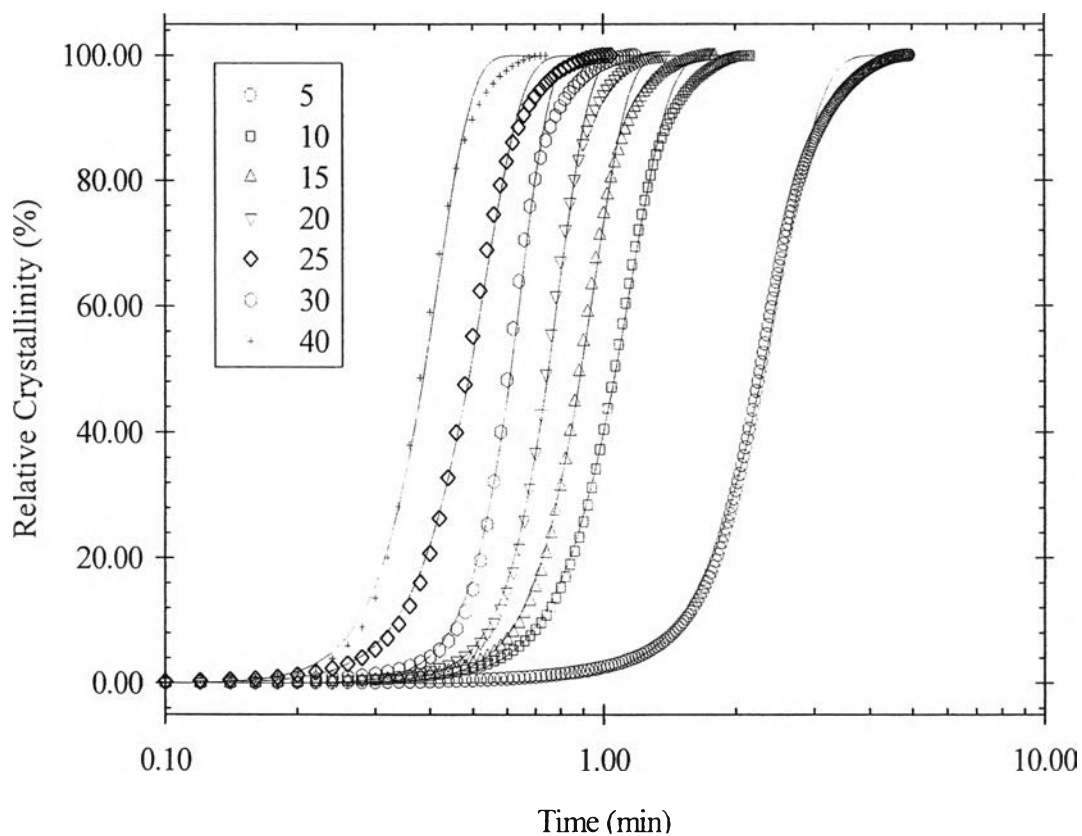
[27]), comparison of the ability of these resins to start crystallizing has to be carried out on a normalized temperature scale, i.e. the degree of undercooling ΔT, not the absolute temperature scale. In so doing, the values of ΔT_{onset} (i.e. $\Delta T_{onset} = T_m^0 - T_{0.01}$) for all resins and cooling conditions studied were calculated and the results are summarized in Table 5.2. Evidently, for any given cooling condition, the ΔT values that these different sPP resins started crystallizing were practically similar. For instance, the ΔT_{onset} values of these resins when being cooled at $10^{\circ}C$ min^{-1} were almost identical to one another (i.e. $56.5^{\circ}C$ for sPP#9, $56.1^{\circ}C$ for sPP#10, $55.0^{\circ}C$ for sPP#11, $54.0^{\circ}C$ for sPP#12, $52.2^{\circ}C$ for sPP#13, and $55.9^{\circ}C$ for sPP#14, respectively).

Figure 5.1(b) Subsequent melting endotherm of sPP#10 after non-isothermal melt-crystallization at corresponding cooling rates. The subsequent melting endotherm was recorded at a heating rate of $20^{\circ}C$ min^{-1}

Table 5.2 Characteristic data from non-isothermal melt-crystallization exotherms for sPP# 9 to sPP#14

| ϕ (°C min^{-1})	$T_{0.01}$ (°C)	T_p (°C)	$T_{0.99}$ (°C)	ΔT_{onset} (°C)	$T_{0.01}$ (°C)	T_p (°C)	$T_{0.99}$ (°C)	ΔT_{onset} (°C)
sPP#9					*sPP#10*			
5	92.2	88.5	85.4	52.0	105.4	100.5	96.2	50.6
10	87.7	83.2	79.3	56.5	99.9	95.5	91.1	56.1
15	84.0	78.7	74.1	60.2	96.0	91.5	86.9	60.0
20	81.4	75.3	69.6	62.8	93.7	88.9	84.3	62.3
25	78.5	71.2	66.3	65.7	91.4	86.6	81.5	64.6
30	76.9	68.4	64.2	67.3	89.2	83.9	78.7	66.8
40	68.5	63.9	59.6	75.7	85.6	79.9	73.8	70.4
sPP#11					*sPP#12*			
5	110.7	106.2	101.6	49.0	93.3	89.3	85.0	49.0
10	104.7	100.3	96.1	55.0	88.3	83.5	79.0	54.0
15	101.2	96.7	92.2	58.5	84.5	78.7	73.9	57.8
20	99.3	94.6	90.2	60.4	81.9	75.9	70.7	60.4
25	97.2	92.4	87.7	62.5	78.9	72.0	65.9	63.4
30	94.8	89.9	84.7	64.9	75.4	68.4	61.7	66.9
40	91.3	85.9	80.4	68.4	71.4	61.9	55.5	70.9
sPP#13					*sPP#14*			
5	104.0	99.4	94.3	47.1	106.8	103.0	99.6	50.2
10	98.9	94.3	89.5	52.2	101.1	97.2	93.3	55.9
15	95.4	90.7	85.5	55.7	97.7	93.5	89.8	59.3
20	93.6	88.3	83.0	57.5	95.2	90.6	86.7	61.8
25	90.6	84.9	79.7	60.5	93.2	88.3	83.7	63.8
30	88.5	82.9	76.8	62.6	90.5	84.9	79.6	66.5
40	84.9	78.6	71.6	66.2	86.9	80.6	75.1	70.1

Figure 5.2(a) Relative crystallinity as a function of time of sPP#11 observed for seven different cooling rates, ranging from 5 to 40oC min-1. The raw experimental data are shown as various geometrical points; whereas the model predictions based on Avrami model are shown as solid lines.

The data can be further analyzed by converting the temperature scale of the $\theta(T)$ curves into the time scale, using Eq. (5.2), to obtain the relative crystallinity as a function of time $\theta(t)$. The converted curves for sPP#11 are illustrated in Fig. 5.2 (viz. the raw data are shown as various geometrical points). According to Fig. 5.2, It is clear that the faster the cooling rate, the shorter the time required for the completion of the crystallization process. Other sPP resins also exhibited a similar behavior. It is worth noting that these $\theta(t)$ curves do not include the apparent incubation period Δt_{inc}, which is

defined as a time period during which the polymer isstill in its molten state [viz. $\Delta t_{inc} = \left(T_f - T_{onset}\right)/\phi$, where T_f is the fusion temperature or the temperature where a polymer sample is brought to melt, T_{onset} is the actual temperature where the sample begins to crystallize, and ϕ is the cooling rate]. The Δt_{inc} values were calculated based on a T_f value of 190°C and are summarized in Table 5.3. For a given sPP resin, the Δt_{inc} value was found to monotonically decrease with increasing cooling rate.
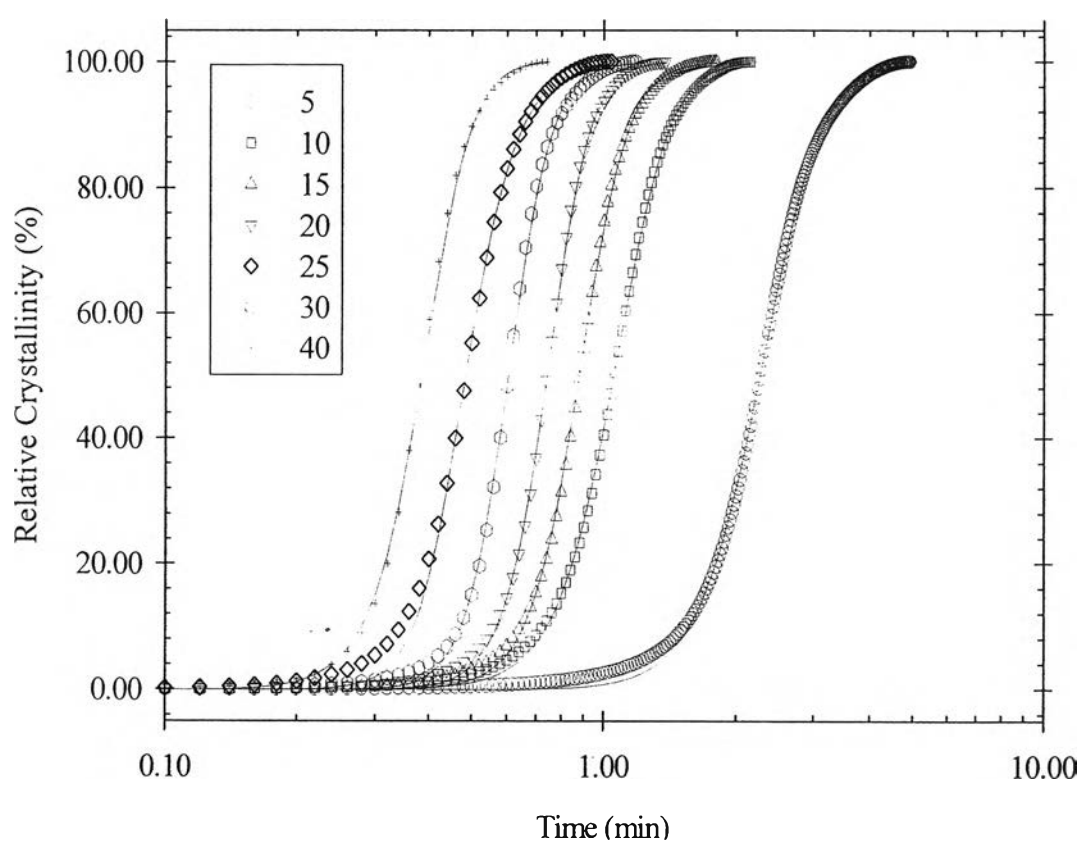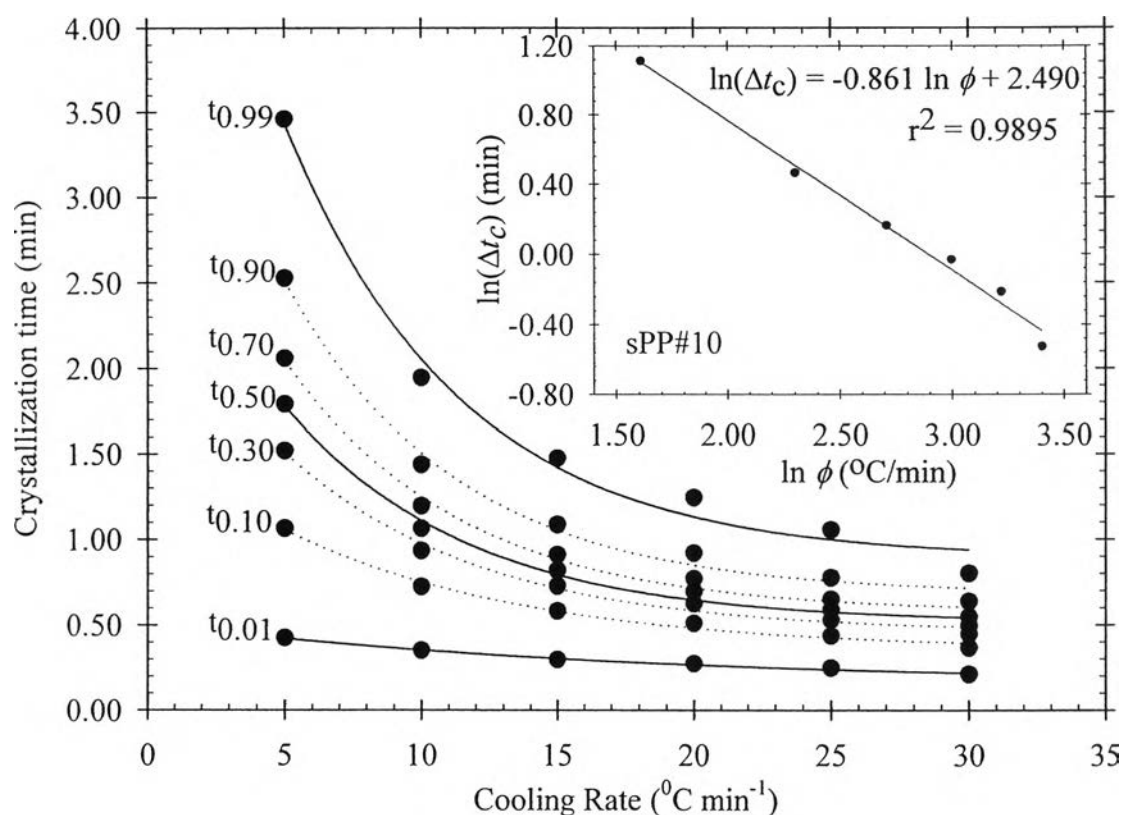

Figure 5.2(b) Relative crystallinity as a function of time of sPP#11 observed for seven different cooling rates, ranging from 5 to 40oC min-1. The raw experimental data are shown as various geometrical points; whereas the model predictions based on Urbanovici-Segal model are shown as solid lines.

Figure 5.3 Crystallization time at various relative crystallinity values as a function of cooling rate for sPP#10. The inset figure shows a relationship between apparent total crystallization period and cooling rate in a log-log plot.

In order to quantify the bulk kinetics of the nonisothermal melt-crystallization process, the crystallization time at an arbitrary relative crystallinity (i.e. t_h) can be determined from the $\theta(t)$ curves. The t_h values (after exclusion of the apparent incubation period Δt_{inc}) for various values of the relative crystallinity θ (i.e. at the θ values of 0.01, 0.1, 0.3, 0.5, 0.7, 0.9, and 0.99, respectively) for all of the sPP resins studied are summarized in Table 5.3. Fig. 5.3 shows plots of t_h as a function of cooling rate for sPP#10. It should be noted that $t_{0.01}$ and $t_{0.99}$ values are qualitative measures of the beginning and the ending of the crystallization process. From the $t_{0.01}$ and $t_{0.99}$ values, the apparent total crystallization period Δt_c can be calculated (i.e. $\Delta t_c = t_{0.99} - t_{0.01}$) and

the results are summarized in Table 5.3. Clearly, the way in which the th value for a given value of θ and the Δt_c value were all found to decrease with increasing cooling rate suggests that nonisothermal melt-crystallization proceeds faster with increasing cooling rate. In an attempt to further analyze the results obtained, plots of $\ln(\Delta t_c)$ against $\ln(\phi)$ (shown as the inset in Fig. 5.3 for sPP#10) and of $\ln(t_\theta)$ against $\ln(\phi)$ (shown in Fig. 5.4 for sPP#10) were carried out. The linearity of these plots is evident. Table 5.4 summarizes values of the y-intercept and the slope obtained from these plots for all of the sPP resins investigated. Interestingly, for a given resin, the y-intercept value was found to increase with increasing θ, while the slope of these different plots was found to be quite similar.

Table 5.3 Quantitative analysis of the relative crystallinity functions of time which were converted from non-isothermal melt-crystallization of sPP#9 to sPP#14

| ϕ ($^{\circ}$C min^{-1})	Δt_{inc} (min)	t_θ (min)							Δt_c (min)
		$\theta=$ 0.01	$\theta=$ 0.1	$\theta=$ 0.3	$\theta=$ 0.5	$\theta=$ 0.7	$\theta=$ 0.9	$\theta=$ 0.99	
sPP#9									
5	18.60	0.59	1.13	1.45	1.65	1.85	2.17	2.81	2.22
10	9.58	0.46	0.76	0.95	1.07	1.19	1.39	1.85	1.39
15	6.62	0.33	0.53	0.67	0.77	0.85	0.98	1.21	0.88
20	5.08	0.25	0.43	0.55	0.63	0.71	0.82	1.04	0.79
25	4.16	0.20	0.37	0.48	0.55	0.62	0.72	0.97	0.77
30	3.52	0.17	0.31	0.41	0.48	0.53	0.60	0.74	0.57
sPP#10									
5	16.08	0.42	1.06	1.52	1.79	2.06	2.53	3.46	3.03
10	8.38	0.35	0.72	0.93	1.06	1.19	1.44	1.94	1.59
15	5.74	0.30	0.58	0.73	0.82	0.91	1.09	1.47	1.18
20	4.30	0.27	0.51	0.62	0.69	0.77	0.92	1.24	0.97
25	3.54	0.25	0.44	0.53	0.59	0.65	0.78	1.05	0.81
30	3.02	0.21	0.37	0.44	0.49	0.55	0.64	0.80	0.59

Table 5.3 Quantitative analysis of the relative crystallinity functions of time which were converted from non-isothermal melt-crystallization of sPP#9 to sPP#14 (*continued*)

ϕ (°C min^{-1})	Δt_{inc} (min)	t_θ (min)							Δt_c (min)
		$\theta=$ 0.01	$\theta=$ 0.1	$\theta=$ 0.3	$\theta=$ 0.5	$\theta=$ 0.7	$\theta=$ 0.9	$\theta=$ 0.99	
	sPP#11								
5	14.30	0.78	1.72	2.19	2.47	2.75	3.31	4.25	3.46
10	7.78	0.45	0.84	1.05	1.18	1.31	1.55	2.02	1.57
15	5.26	0.37	0.70	0.85	0.95	1.04	1.25	1.77	1.40
20	3.98	0.30	0.58	0.70	0.77	0.84	1.02	1.40	1.10
25	3.36	0.21	0.38	0.47	0.53	0.59	0.70	0.94	0.73
30	2.84	0.18	0.35	0.43	0.48	0.54	0.65	0.88	0.70
	sPP#12								
5	18.10	0.84	1.47	1.84	2.09	2.35	2.87	3.77	2.93
10	9.42	0.55	0.88	1.09	1.22	1.36	1.63	2.24	1.69
15	6.54	0.36	0.58	0.74	0.84	0.93	1.07	1.32	0.96
20	5.06	0.23	0.42	0.54	0.62	0.70	0.82	1.08	0.85
25	4.16	0.18	0.35	0.46	0.53	0.60	0.72	0.95	0.77
30	3.58	0.14	0.28	0.38	0.44	0.50	0.59	0.71	0.58
	sPP#13								
5	15.68	0.54	1.44	2.08	2.43	2.80	3.57	4.41	3.87
10	8.50	0.37	0.72	0.93	1.06	1.20	1.43	1.87	1.50
15	5.84	0.31	0.54	0.69	0.78	0.88	1.06	1.37	1.06
20	4.40	0.26	0.47	0.59	0.67	0.76	0.92	1.21	0.95
25	3.68	0.20	0.35	0.44	0.50	0.57	0.69	0.91	0.71
30	3.12	0.19	0.31	0.38	0.44	0.49	0.59	0.73	0.53
	sPP#14								
5	15.70	0.59	1.13	1.48	1.70	1.94	2.45	3.32	2.73
10	8.38	0.35	0.61	0.78	0.90	1.01	1.22	1.60	1.25
15	5.82	0.23	0.40	0.51	0.58	0.66	0.78	0.98	0.75
20	4.46	0.19	0.33	0.42	0.48	0.54	0.66	0.92	0.73
25	3.62	0.17	0.29	0.37	0.43	0.48	0.58	0.75	0.58
30	3.06	0.15	0.29	0.37	0.43	0.48	0.59	0.82	0.66

Table 5.4 y-intercept, slope, and the r^2 values of regression lines drawn through plots of $\ln(t_\theta)$ against $\ln(\phi)$ for various relative crystallinity values

θ	y-intercept (min)	slope (min^2 °C^{-1})	r^2	y-intercept (min)	slope (min^2 °C^{-1})	r^2
sPP#9				sPP#10		
0.01	0.77	-0.730	0.9570	-0.22	-0.374	0.9678
0.1	1.33	-0.726	0.9938	1.00	-0.573	0.9921
0.3	1.54	-0.711	0.9972	1.48	-0.664	0.9966
0.5	1.65	-0.701	0.9980	1.69	-0.697	0.9973
0.7	1.75	-0.699	0.9982	1.87	-0.720	0.9974
0.9	1.93	-0.711	0.9974	2.11	-0.743	0.9963
0.99	2.23	-0.727	0.9835	2.48	-0.771	0.9900
Δt_c	1.96	-0.726	0.9710	2.49	-0.861	0.9895
sPP#11				sPP#12		
0.01	1.06	-0.795	0.9788	1.64	-1.039	0.9674
0.1	1.92	-0.865	0.9763	1.96	-0.938	0.9926
0.3	2.19	-0.888	0.9816	2.09	-0.894	0.9963
0.5	2.32	-0.895	0.9843	2.17	-0.875	0.9974
0.7	2.43	-0.899	0.9858	2.27	-0.867	0.9980
0.9	2.61	-0.896	0.9839	2.49	-0.885	0.9978
0.99	2.81	-0.862	0.9730	2.84	-0.920	0.9889
Δt_c	2.62	-0.879	0.9692	2.50	-0.888	0.9804
sPP#13				sPP#14		
0.01	0.36	-0.588	0.9805	0.69	-0.769	0.9929
0.1	1.68	-0.841	0.9898	1.35	-0.798	0.9720
0.3	2.14	-0.916	0.9871	1.63	-0.808	0.9726
0.5	2.31	-0.929	0.9867	1.77	-0.811	0.9728
0.7	2.46	-0.940	0.9857	1.90	-0.815	0.9715
0.9	2.73	-0.967	0.9804	2.15	-0.834	0.9612
0.99	2.95	-0.953	0.9833	2.42	-0.828	0.9428
Δt_c	2.93	-1.034	0.9789	2.23	-0.843	0.9230
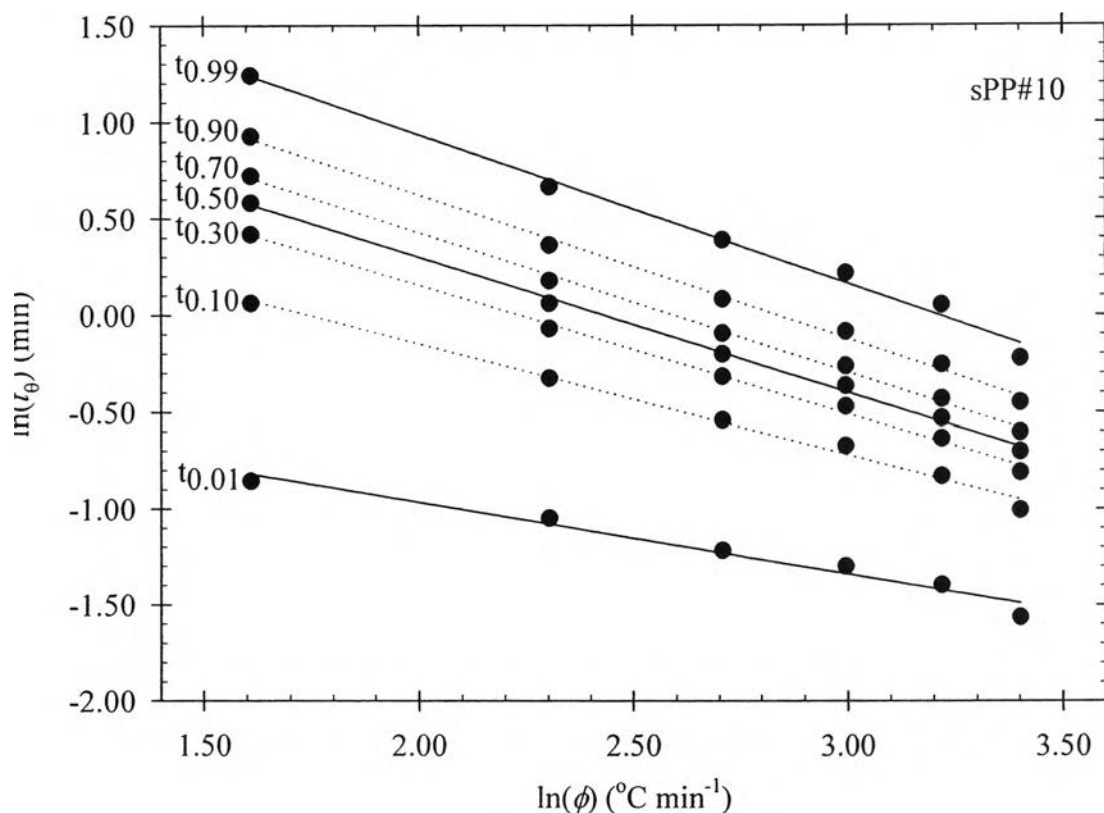
Figure 5.4 Relationship between crystallization time at various relative crystallinity values and cooling rate in a log-log plot for sPP#10.

Subsequent melting endotherms of sPP#10 after non-isothermal melt-crystallization at seven different cooling rates, ranging from 5 to 40°C min^{-1}, are shown in Fig. 5.1(b). These exotherms were recorded at a heating rate of 20°C min^{-1}. For sPP#10, double melting endotherms were observed for non-isothermal meltcrystallization at cooling rates greater than or equal to 10°C min^{-1}, while a single melting endotherm was observed at 5°C min^{-1} or lower. Evidently, the size and sharpness of these melting peaks depended on the cooling rate used to crystallize the sample. Generally, for a given sPP resin, the low-temperature melting peak was found to increase in its size and sharpness and move towards a higher temperature become

smaller with decreasing cooling rate or even disappeared altogether at some low enough cooling rates. Table 5.5 summarizes values of the lowtemperature and the high-temperature melting peaks for all of the sPP resins investigated. Clearly, the peak value of the low-temperature melting peak (i.e. T_{ml}), for a given sPP resin, was found to increase with decreasing cooling rate, while the peak value of the high-temperature melting peak (i.e. T_{mh}) was found to increase very slightly with decreasing cooling rate and even disappeared altogether at some low enough cooling rate. These observations should be a direct result of the increased stability of the primary crystallites formed during cooling at low cooling rates [28].

Table 5.5 Characteristic data of subsequent melting endotherms after non-isothermal melt-crystallization for sPP#9 to sPP#14

ϕ (°C min^{-1})	T_{ml} (°C)	T_{mh} (°C)	T_{ml} (°C)	T_{mh} (°C)	T_{ml} (°C)	T_{mh} (°C)
	sPP#9		sPP#10		sPP#11	
5	124.0	132.0	135.0	-	144.1	-
10	122.7	132.0	134.0	140.4	141.4	-
15	121.4	132.1	133.1	140.4	140.7	146.4
20	120.4	131.4	132.1	140.1	139.7	145.7
25	119.4	131.4	131.4	139.7	139.4	145.7
30	119.4	131.1	131.1	139.7	138.7	145.7
40	118.4	130.7	130.4	139.7	138.4	145.7
	sPP#12		sPP#13		sPP#14	
5	125.7	-	135.0	-	141.0	-
10	124.0	130.7	133.7	-	139.7	-
15	123.1	130.4	132.1	-	138.4	-
20	122.1	130.1	132.1	-	138.4	-
25	121.4	129.7	131.4	137.7	137.7	-
30	120.7	129.7	131.1	137.7	137.4	-
40	120.0	129.7	130.7	137.7	136.7	143.4

5.5.2 Non-Isothermal Melt-Crystallization Kinetics

5.5.2.1 Avrami Analysis

Analysis of the non-isothermal melt-crystallization data according to the Avrami model can be done by fitting the $\theta(t)$ functions, such as those shown in Fig. 5.2 for sPP#11, to Eq. (5.3) directly. The obtained values of the Avrami kinetic parameters (i.e. n_A and K_A) along with the r^2 parameter, signifying the quality of the fitting, for all of the sPP resins studied are summarized in Table 5.6. According to the values of the r^2 parameter, the non-isothermal melt-crystallization data of these sPP resins were well described by the Avrami model (see Fig. 5.2(a): the predicted curves based on the Avrami model, shown as solid lines, versus the experimental data, shown as various geometrical points). For all of the sPP resins studied, n_A was found to range from ca. 3.2 to 6.7. Specifically, it ranged from ca. 3.8 to 5.6 for sPP#9, from ca. 4.5 to 6.7 for sPP#10, from ca. 4.3 to 6.4 for sPP#11, from ca. 3.9 to 6.5 for sPP#12, from ca. 3.2 to 5.3 for sPP#13, and from ca. 3.5 to 4.4 for sPP#14, respectively. The values of n_A found in this work were quite comparable with the values of ca. 2.4 to 5.3 which were reported in a previous work [29]. For a given sPP resin, K_A was found to increase with increasing cooling rate, as expected.

5.5.2.2 Urbanovici-Segal Analysis

Analysis of the non-isothermal melt-crystallization data according to the Urbanovici–Segal model can be done by fitting the $\theta(t)$ functions, such as those shown in Fig. 5.2 for sPP#11, to Eq. (5.4) directly. The obtained values of the Urbanovici–Segal kinetic parameters (i.e. n_{US}, K_{US} and r) along with the r^2 parameter for all of the sPP resins studied are summarized in Table 5.7. Comparison of the values of the r^2 parameter summarized in Tables 5.6 and 5.7 suggests that Urbanovici–Segal model provided a much better description to the non-isothermal melt-crystallization data of these sPP resins than did the Avrami model. Fig. 5.2(b) shows, in comparison, the predicted curves based on the Urbanovici–Segal model (i.e. the solid lines) versus the experimental data (i.e. shown as various geometrical points) for sPP#11. For all of the sPP resins studied, n_{US} was found to range from ca.

3.8 to 9.0. Specifically, it ranged from ca. 4.0 to 5.9 for sPP#9, from ca. 5.3 to 9.0 for sPP#10, from ca. 5.8 to 9.0 for sPP#11, from ca. 4.4 to 8.8 for sPP#12, from ca. 3.8 to 7.0 for sPP#13, and from ca. 4.1 to 5.4 for sPP#14, respectively. For a given sPP resin, K_{US} was found, in a similar manner to K_A, to increase with increasing cooling rate, as expected.

Table 5.6 Non-isothermal melt-crystallization kinetic parameters for sPP# 9 to sPP#14 based on Avrami analysis

ϕ ($^{\circ}$C min^{-1})	K_A (min^{-1})	n_A	r^2	K_A (min^{-1})	n_A	r^2
	sPP#9			sPP#10		
5	0.73	3.78	0.9998	0.37	5.95	0.9977
10	1.15	3.90	0.9997	0.92	4.46	0.9993
15	1.46	4.11	0.9999	1.13	5.14	0.9990
20	1.42	4.75	0.9996	1.41	5.25	0.9987
25	1.63	4.88	0.9998	1.36	6.66	0.9985
30	1.87	4.81	0.9998	1.69	6.25	0.9990
40	2.75	5.60	0.9998	2.59	5.00	0.9991
	sPP#11			sPP#12		
5	0.40	4.31	0.9983	0.57	3.23	0.9993
10	0.87	4.73	0.9990	0.75	5.05	0.9997
15	1.05	5.50	0.9988	1.02	5.26	0.9998
20	1.26	6.14	0.9988	1.55	4.44	0.9999
25	1.88	4.83	0.9985	2.07	4.29	0.9997
30	1.54	6.40	0.9980	2.42	4.08	0.9999
40	2.40	5.42	0.9983	3.12	3.86	0.9965
	sPP#13			sPP#14		
5	0.40	3.23	0.9992	0.55	4.27	0.9987
10	0.75	5.05	0.9998	1.06	4.39	0.9989
15	1.02	5.26	0.9999	1.92	3.53	0.9994
20	1.55	4.44	0.9999	2.38	3.60	0.9995
25	2.07	4.29	0.9999	2.46	3.99	0.9994
30	2.42	4.08	1.0000	2.50	4.09	0.9992
40	3.12	3.86	0.9997	3.16	4.08	0.9996

Table 5.7 Non-isothermal melt-crystallization kinetic parameters for sPP# 9 to

sPP#14 based on Urbanovici-Segal analysis

ϕ ($^{\circ}$C min^{-1})	K_A (min^{-1})	n_A	r	r^2	K_A (min^{-1})	n_A	r	r^2
	sPP#9				sPP#10			
5	0.73	3.78	1.19	0.9998	0.37	5.95	1.52	0.9977
10	1.15	3.90	1.30	0.9997	0.92	4.46	1.46	0.9993
15	1.46	4.11	1.16	0.9999	1.13	5.14	1.64	0.9990
20	1.42	4.75	1.38	0.9996	1.41	5.25	1.79	0.9987
25	1.63	4.88	1.18	0.9998	1.36	6.66	1.92	0.9985
30	1.87	4.81	1.17	0.9998	1.69	6.25	1.64	0.9990
40	2.75	5.60	1.07	0.9998	2.59	5.00	1.52	0.9991
	sPP#11				sPP#12			
5	0.40	4.31	1.77	0.9983	0.57	3.23	1.43	0.9993
10	0.87	4.73	1.60	0.9990	0.75	5.05	1.27	0.9997
15	1.05	5.50	1.79	0.9988	1.02	5.26	1.19	0.9998
20	1.26	6.14	1.76	0.9988	1.55	4.44	1.14	0.9999
25	1.88	4.83	2.28	0.9985	2.07	4.29	2.51	0.9997
30	1.54	6.40	2.01	0.9980	2.42	4.08	1.47	0.9999
40	2.40	5.42	1.55	0.9983	3.12	3.86	1.74	0.9965
	sPP#13				sPP#14			
5	0.40	3.23	1.34	0.9992	0.55	4.27	1.63	0.9987
10	0.75	5.05	1.63	0.9998	1.06	4.39	1.59	0.9989
15	1.02	5.26	1.81	0.9999	1.92	3.53	1.43	0.9994
20	1.55	4.44	1.56	0.9999	2.38	3.60	1.30	0.9995
25	2.07	4.29	1.43	0.9999	2.46	3.99	1.41	0.9994
30	2.42	4.08	1.33	1.0000	2.50	4.09	1.47	0.9992
40	3.12	3.86	1.52	0.9997	3.16	4.08	1.45	0.9996

5.5.2.3 Ozawa Analysis

By simply replacing t in Eq. (5.3) with T/ϕ, Ozawa [17] was able to extend the Avrami model to describe non-isothermal crystallization kinetics for a semi-crystalline polymer. In this approach, the raw data are the $\theta(T)$ functions. Data analysis according to this model can be accomplished through a plot of $\ln[-\ln(1 - \theta(T))]$

versus $\ln(\phi)$ for a fixed temperature, where n_O is taken as the negative value of the slope and K_O is taken as the antilogarithmic value of the ratio of the y-intercept and n_O [i.e. $K_O = \exp(y - \text{intercept}/n_O)$]. Fig. 5.5 shows typical Ozawa plots from the raw data taken for sPP#13 within a temperature range of 80 to 94°C, while Table 5.8 summarizes the Ozawa kinetic parameters (i.e. n_O and K_O), including the r^2 parameter for all of the sPP resins investigated. Based on the values of the r^2 parameter obtained, it was found that Ozawa model was satisfactory in describing the non-isothermal melt-crystallization data of these sPP resins. For all of the sPP resins investigated, n_O was found to range from ca. 1.9 to 6.7. Specifically, it was found to range from ca. 4.2 to 6.7 for sPP#9, from ca. 3.3 to 5.2 for sPP#10, from ca. 3.8 to 5.6 for sPP#11, from ca. 2.9 to 6.6 for sPP#12, from ca. 1.9 to 5.0 for sPP#13, and from ca. 2.6 to 6.1 for sPP#14, respectively. For a given sPP resin, K_O was found to decrease with increasing temperature, as normally would for crystallization in the nucleation-controlled region.

5.5.2.4 Ziabicki's Kinetic Crystallizability Analysis

Analysis according to the modified first-order Ziabicki's kinetic equation (i.e. Eq. (5.9)) can be carried out by differentiating a $\theta(T)$ function with respect to temperature in order to obtain the temperature-derivative relative crystallinity as a function of temperature $(d\theta/dT)_\phi$. Once the $(d\theta/dT)_\phi$ function is obtained, various kinetic parameters [i.e. the maximum crystallization rate $(d\theta/dT)_{\phi,\max}$ and the width at half-height of the $(d\theta/dT)_\phi$ function of D_ϕ] can be obtained and the cooling rate-dependent kinetic crystallizability index $G_{Z,\phi}$ can be calculated according to Eq. (5.9). Table 5.9 summarizes values of $T_{\max,\phi}$ (i.e. the temperature at the maximum crystallization rate which can be obtained from the $(d\theta/dT)_\phi$ function), $(d\theta/dT)_{\phi,\max}$, D_ϕ, and G_Z for all the sPP resins investigated. It should be noted that the values of $T_{\max,\phi}$ listed in Table 5.9 and T_p (i.e. the temperature at the maximum crystallization rate as determined from the raw non-isothermal melt-crystallization exotherms) listed in Table 5.1 are practically the same. According to Table 5.9, the value of $T_{\max,\phi}$ was found to decrease, while those

of $(d\theta/dT)_{\phi,\text{max}}$, D_ϕ, and $G_{Z,\phi}$ (the results not shown) were basically found to increase, with increasing cooling rate. Normalization of $G_{Z,\phi}$ with ϕ gave the value of G_Z. It is evident that the normalized G_Z values obtained for different cooling rates for a given sPP resin were almost identical. For all of the sPP resins investigated, G_Z was found to vary between ca. 0.88 and 0.95, which is in accord with the values of between ca. 0.93 and 1.40 reported previously [29].
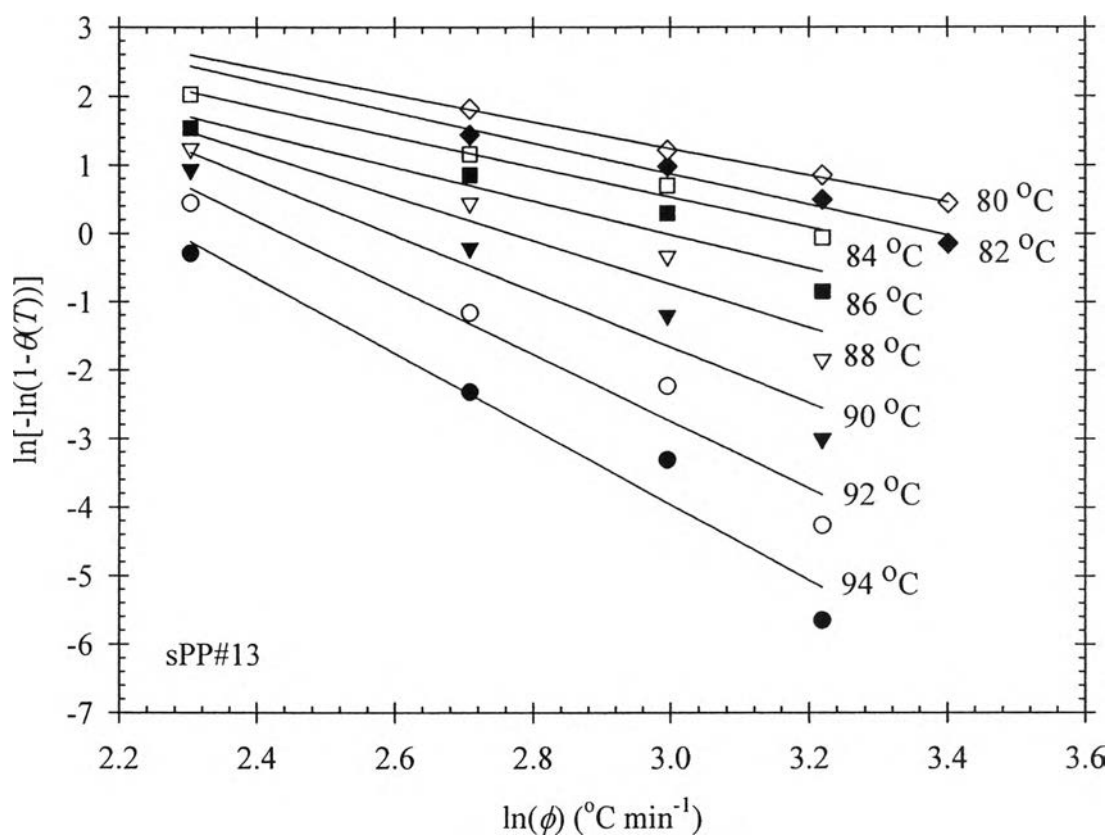
Figure 5.5 Typical Ozawa analysis based on non-isothermal melt-crystallization data of sPP#13.

Table 5.8 Non-isothermal melt-crystallization kinetic parameters for sPP# 9 to sPP#14 based on Ozawa analysis

Temperature (^{o}C)	K_O (min^{-1})	n_O	r^2	Temperature (^{o}C)	K_O (min^{-1})	n_O	r^2
sPP#9				sPP#10			
86	6.12	5.42	0.9642	102	4.08	4.97	0.9983
84	8.94	6.69	0.9997	100	5.26	5.18	0.9546
82	10.56	6.28	0.9948	98	6.38	5.09	0.9381
80	12.10	5.53	0.9846	96	8.84	5.22	0.9906
78	13.76	4.65	0.9593	94	10.58	5.05	0.9952
76	17.34	5.55	0.9943	92	12.36	4.67	0.9856
74	19.67	4.87	0.9904	90	14.37	4.07	0.9527
72	22.98	4.92	0.9980	88	16.97	3.29	0.9141
70	26.16	4.18	1.0000	86	21.71	3.34	0.9288
sPP#11				sPP#12			
110	3.21	5.59	0.9919	86	6.49	6.58	0.8976
108	3.38	4.09	0.9756	84	7.16	4.83	0.9331
106	4.28	3.83	0.9754	82	8.27	3.98	0.9129
104	6.51	5.01	0.8629	80	12.34	6.19	0.9315
102	7.85	4.74	0.9703	78	13.71	5.07	0.9217
100	9.57	4.53	0.9898	76	15.53	4.20	0.8879
98	11.58	4.35	0.9885	74	18.00	3.46	0.8497
96	13.69	3.90	0.9587	72	21.53	2.87	0.8287
94	17.86	4.27	0.9360	70	25.63	3.81	0.9647
sPP#13				sPP#14			
96	6.41	4.64	0.9047	98	6.88	6.07	0.9127
94	7.36	3.78	0.8981	96	8.16	4.65	0.9290
92	8.81	4.13	0.8103	94	9.70	3.95	0.8186
90	13.40	4.98	0.9244	92	14.41	4.74	0.9296
88	15.45	3.92	0.9110	90	17.09	3.91	0.8844
86	18.50	3.06	0.9121	88	21.00	3.24	0.8737
84	23.35	2.56	0.9582	86	25.76	3.83	0.9425
82	29.69	2.24	0.9689	84	30.55	3.32	0.8884
80	38.01	1.94	0.9973	82	37.49	2.58	0.8924

Table 5.9 Non-isothermal melt-crystallization kinetic parameters for sPP# 9 to sPP#14 based on Ziabicki's kinetic crystallizability analysis

ϕ (°C min^{-1})	$T_{max,\phi}$ (°C)	$(d\theta/dT)_{\phi,max}$ (s^{-1})	D_ϕ (°C)	G_z	$T_{max,\phi}$ (°C)	$(d\theta/dT)_{\phi,max}$ (s^{-1})	D_ϕ (°C)	G_z
sPP#9					sPP#10			
5	88.5	0.017	4.09	0.91	100.6	0.013	5.30	0.89
10	83.2	0.030	4.97	0.94	95.5	0.027	5.18	0.90
15	78.7	0.039	5.86	0.96	91.5	0.039	5.38	0.90
20	75.3	0.042	7.02	0.95	89.0	0.048	5.72	0.88
25	71.2	0.048	7.69	0.95	86.6	0.060	5.99	0.92
30	68.4	0.062	7.35	0.96	83.9	0.065	6.53	0.91
40	63.9	0.087	6.19	0.86	79.9	0.077	7.50	0.92
Average				0.93 ±0.04				0.90 ±0.01
sPP#11					sPP#12			
5	106.2	0.013	5.28	0.88	89.2	0.015	4.88	0.91
10	100.3	0.028	5.04	0.88	83.5	0.026	5.55	0.94
15	96.7	0.039	5.34	0.88	78.7	0.036	6.30	0.96
20	94.9	0.050	5.47	0.88	75.9	0.044	6.68	0.94
25	92.4	0.061	5.77	0.89	72.0	0.047	7.92	0.95
30	89.9	0.064	6.28	0.86	68.4	0.054	8.50	0.98
40	85.9	0.081	7.04	0.91	61.9	0.057	10.26	0.94
Average				0.88 ±0.01				0.95 ±0.02
sPP#13					sPP#14			
5	99.5	0.011	6.08	0.81	103.1	0.018	4.09	0.94
10	94.3	0.027	5.49	0.94	97.2	0.032	4.53	0.92
15	90.5	0.038	5.73	0.93	93.7	0.047	4.71	0.95
20	88.3	0.043	6.47	0.88	90.9	0.056	5.20	0.93
25	84.9	0.052	6.73	0.89	88.3	0.062	5.81	0.92
30	82.9	0.060	7.27	0.93	84.9	0.064	6.70	0.92
40	78.6	0.073	8.17	0.96	81.2	0.078	7.58	0.94
Average				0.91 ±0.05				0.93 ±0.01

5.5.2.5 Effective Energy Barrier for Non-Isothermal Melt-

Crystallization Process

Analysis based on the differential iso-conversional method of Friedman begins with the conversion of a $\theta(T)$ function into a $\theta(t)$ function. The converted $\theta(t)$ function is then differentiated with respect to time to obtain the instantaneous crystallization rate as a function of time $\dot\theta(t)$. A plot according to Eq. (5.10) can then be performed for various values of relative crystallinity ϕ using the data obtained from both $\dot\theta(t)$ and $\theta(T)$ functions and, finally, the effective energy barrier for non-isothermal melt-crystallization process for a given value of ϕ (i.e. ΔE_θ) can be determined from the slope of the plot [i.e. ΔE_θ=-(slope)(R)]. The ΔE_θ values determined for various values of θ, ranging from 0.1 to 0.9 with 0.1 increment, for all of the sPP resins studied are summarized in Table 5.10. Among the various sPP resins investigated, the values of ΔE_θ obtained can be ranked in the following order: sPP#13 < sPP#11 < sPP#10 < sPP#14 < sPP#12 < sPP#9.

Table 5.10 Effective energy barrier for overall non-isothermal melt-crystallization of sPP#9 to sPP#14 based on the differential iso-conversional method of Friedman

Conversion θ	ΔE_θ (kJ mol^{-1})	r^2	ΔE_θ (kJ mol^{-1})	r^2	ΔE_θ (kJ mol^{-1})	r^2
	sPP#9		sPP#10		sPP#11	
0.1	-75.0	0.9398	-121.4	0.9859	-135.5	0.9877
0.2	-65.9	0.9383	-118.8	0.9783	-128.9	0.9869
0.3	-61.0	0.9363	-113.8	0.9744	-123.4	0.9838
0.4	-59.2	0.9409	-108.7	0.9725	-119.5	0.9800
0.5	-59.1	0.9516	-104.5	0.9712	-115.7	0.9751
0.6	-60.3	0.9624	-102.9	0.9706	-113.4	0.9712
0.7	-62.7	0.9706	-99.3	0.9767	-112.4	0.9675
0.8	-66.4	0.9735	-98.4	0.9806	-111.0	0.9579
0.9	-71.6	0.9553	-97.1	0.9634	-102.0	0.9226

Table 5.10 Effective energy barrier for overall non-isothermal melt-crystallization of sPP#9 to sPP#14 based on the differential iso-conversional method of Friedman (*continued*)

Conversion θ	ΔE_θ (kJ mol^{-1})	r^2	ΔE_θ (kJ mol^{-1})	r^2	ΔE_θ (kJ mol^{-1})	r^2
	sPP#12		sPP#13		sPP#14	
0.1	-77.0	0.9401	-139.5	0.9649	-106.0	0.9273
0.2	-71.5	0.9425	-132.1	0.9453	-99.4	0.9296
0.3	-69.4	0.9343	-122.7	0.9417	-94.2	0.9196
0.4	-66.4	0.9306	-115.4	0.9409	-90.8	0.9123
0.5	-66.6	0.9207	-112.9	0.9361	-88.3	0.8966
0.6	-67.5	0.9148	-113.7	0.9279	-87.3	0.8749
0.7	-70.3	0.9131	-117.7	0.9074	-88.7	0.8466
0.8	-77.3	0.9084	-124.3	0.8764	-92.8	0.7957
0.9	-94.1	0.8974	-120.1	0.8592	-90.0	0.6964

5.6 Conclusions

Non-isothermal melt-crystallization and subsequent melting behaviors for six sPP resins having different molecular characteristics were investigated using DSC. The results showed that, for a given sPP resin, the crystallization exotherm became wider and shifted towards a lower temperature with an increase in the cooling rate used. Among all of the sPP resins investigated, the crystallization exotherm of sPP#11, in comparison with other sPP resins, for a given cooling rate was found to locate at the highest temperature range, followed by that of sPP#14, sPP#10, sPP#13, sPP#12, and sPP#9, respectively. The results suggested that, based on the absolute temperature scale, sPP#11 showed the highest tendency, among all of the sPP resins studied, to start crystallizing during a cooling scan. The ability for these resins to start crystallizing was found to be very similar when the difference in the equilibrium melting temperature of these resins was taken into account. The Avrami, Urbanovici–Segal, Ozawa, and Ziabicki models were found to describe the

non-isothermal melt-crystallization data of these sPP resins fairly well. Lastly, the subsequent melting behavior of these sPP resins showed either a single melting endotherm or double melting endotherms. Generally, for a given sPP resin, the low-temperature melting endotherm was found to increase in its size and sharpness and move towards a higher temperature with decreasing cooling rate, while the high-temperature melting endotherm was found to get smaller with decreasing cooling rate or even disappeared altogether at some low enough cooling rates.

5.7 Acknowledgements

5.8 References

[1] G. Natta, I. Pasquon, P. Corradini, M. Peraldo, M. Pegorado, A. Zambelli, Rend. Acd. Naz. Lincei. 28 (1960) 539.

[2] G. Natta, I. Pasquon, A. Zambelli, J. Am. Chem. Soc. 84 (1962) 1488.

[3] J.A. Ewen, R.L. Johns, A. Razavi, J.D. Ferrara, J. Am. Chem. Soc. 110 (1988) 6255.

[4] J. Schardl, L. Sun, S. Kimura, R. Sugimoto, SPE-ANTEC Proceedings, 1995, pp. 3414.

[5] J. Schardl, L. Sun, S. Kimura, R. Sugimoto, J. Plastic Film Sheet 12 (1996) 157.

[6] L. Sun, E. Shamshoum, G. DeKunder, SPE-ANTEC Proceedings, 1996, pp. 1965.

[7] M. Gownder, SPE-ANTEC Proceedings, 1995, pp. 2275.

[8] R.K. Sura, P. Desai, A.S. Abhiraman, SPE-ANTEC Proceedings, 1999, pp. 1764.

[9] M. Avrami, J. Chem. Phys. 7 (1939) 1103.

[10] M. Avrami, J. Chem. Phys. 8 (1940) 212.

[11] M. Avrami, J. Chem. Phys. 9 (1941) 177.

[12] B. Wunderlich, Macromolecular Physics, vol. 2 Academic Press, New York, 1976, pp. 147.

[13] P. Supaphol, J. Appl. Polym. Sci. 78 (2000) 338.

[14] Q.X. Zhang, Z.H. Zhang, H.F. Zhang, Z.S. Mo, J. Polym. Sci.—Polym. Phys. 40 (2002) 1784.

[15] E. Urbanovici, E. Segal, Thermochim. Acta 171 (1990) 87.

[16] U.R. Evans, Trans. Faraday Soc. 41 (1945) 365.

[17] T. Ozawa, Polymer 12 (1971) 150.

[18] A. Ziabicki, Appl. Polym. Symp. 6 (1967) 1.

[19] A. Ziabicki, Polymer 12 (1967) 405.

[20] A. Ziabicki, Fundamentals of Fiber Spinning, John Wiley & Sons, New York, 1976, pp. 112–114.

[21] H. Friedman, J. Polym. Sci. C6 (1964-65) 183.

[22] S. Vyazovkin, J. Comput. Chem. 18 (1997) 393.

[23] S. Vyazovkin, J. Comput. Chem. 22 (2001) 178.

[24] S. Vyazovkin, Macromol. Rapid Commun. 23 (2002) 771.

[25] P. Supaphol, J.E. Spruiell, J. Appl. Polym. Sci. 75 (2000) 337.

[26] P. Supaphol, J.S. Lin, Polymer 42 (2001) 9617.

[27] P. Thanomkiat, R.A. Phillips, P. Supaphol, Eur. Polym. J. 40 (2004) 1671.

[28] P. Supaphol, J. Appl. Polym. Sci. 82 (2001) 1083.

[29] P. Supaphol, J. Appl. Polym. Sci. 78 (2000) 338.